Supporting Information

Multi-material direct ink writing (DIW) for complex 3D metallic structures with removable supports

Chao Xu,[a] Bronagh Quinn,[a] Gilles L'Espérance,[b] Louis Laberge Lebel[a] and Daniel Therriault*[a]

[a]Department of Mechanical Engineering, Polytechnique Montreal, Montreal, QC, Canada

[b]Department of Metallurgy Engineering, Polytechnique Montreal, Montreal, QC, Canada

E-mail: daniel.therriault@polymtl.ca

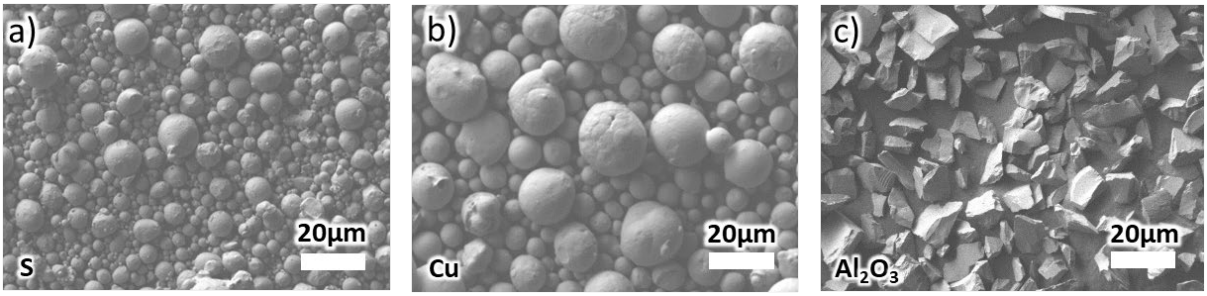

Figure S1. SEM images of a) steel, b) copper and c) alumina micro particles.

The steel and copper particles are spherical, while the alumina particles are irregular in shape featuring sharp corners.

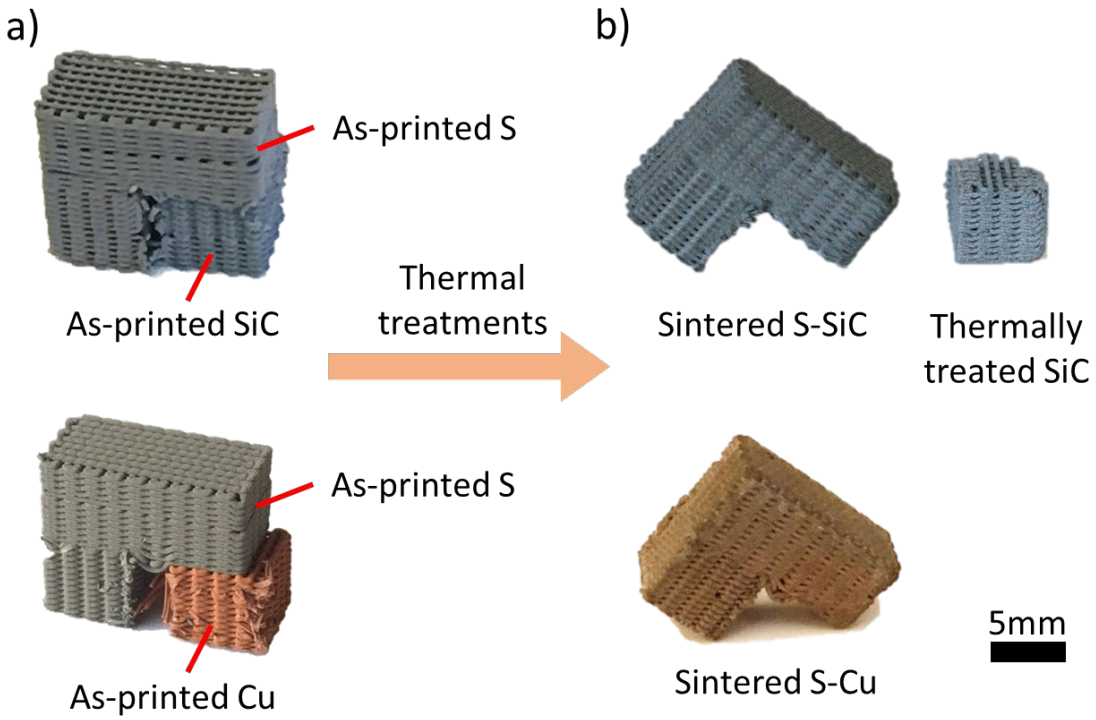

Figure S2. An inverted "L" shape printed from steel ink with a cubic support structure printed from silica carbide or copper ink through the presented multi-material DIW method. (a) As-printed S-SiC and S-Cu inverted "L" shape structures and (b) thermally treated S-SiC and S-Cu inverted "L" shape structures

In our preliminary experiments, we printed an inverted "L" shape, which is relatively a simple geometry, but impossible to print by DIW inversely without a support material due to the large overhang feature. As shown in **Figure S2**, the inverted "L" shape sample is printed using our multi-material approach. The inverted "L" shape is made from steel ink while the support structure is made from a SiC or Cu inks. The inverted "L" structures were successfully sintered without the collapse of the large overhang feature. It proves that our method can build 3D metallic structures featuring overhang structures with easily removable the support materials.

Following our inverted "L" preliminary experiments, we printed the femur bone structure, which is a more complex geometry and features moderate overhangs and bridges. We selected the femur geometry for our manuscript, but we will add the inverted "L" geometry in the Supplementary Information section.

At the beginning, we use silica carbide as the ceramic material. But we found that it is not as suitable as alumina in our case. Because the silica carbide will infiltrate into the steel structure at high temperature during the thermal treatment, which lowers the melting temperature of the steel and increases the risk of the melting of the steel structure. Therefore, we switch to alumina

which is chemically and physically stable at high temperature. As we've already prove that our method works using silica carbide, we skip the inverted "L" shape step and print the femur structure directly for alumina.

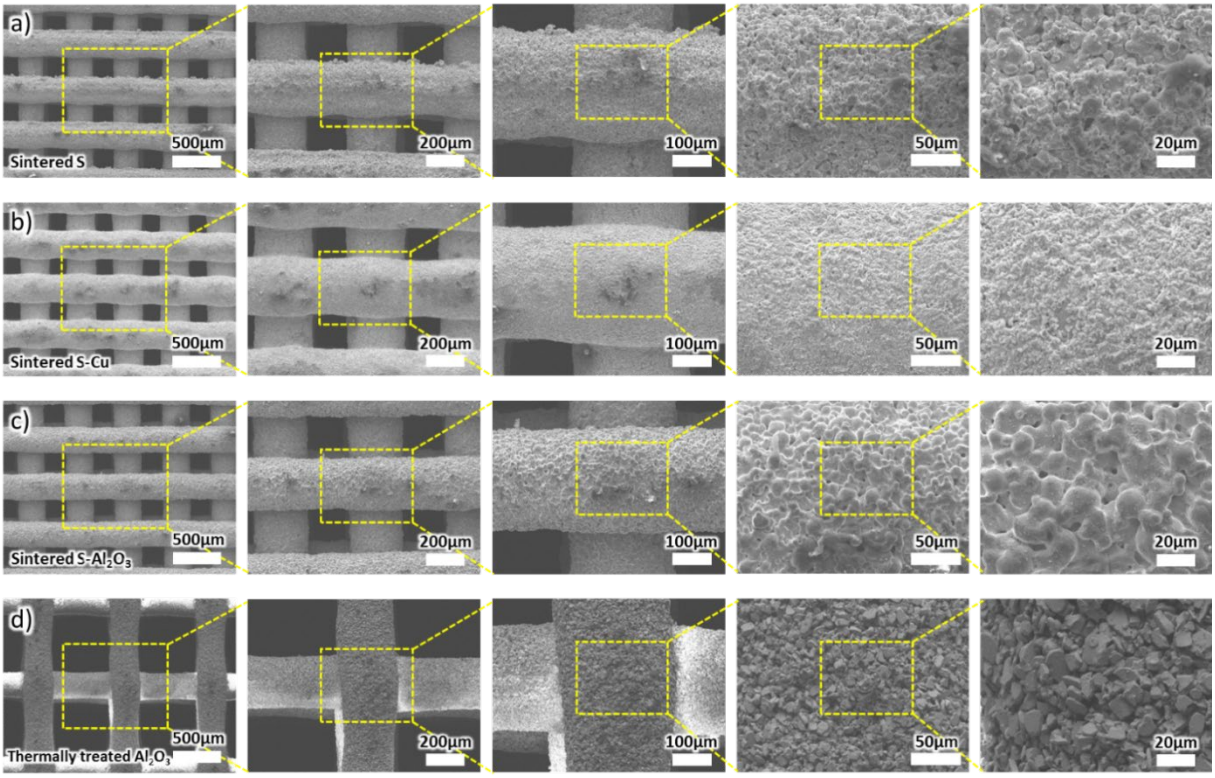

Figure S3. SEM images of the top layer of the sintered (thermally treated) scaffolds at different magnifications: (a) sintered S, (b) sintered S-Cu, (c) sintered S-Al_2O_3, and (d) thermal treated Al_2O_3.

The sintered (thermally treated) scaffolds preserve the original structure and the filaments are orderly structured. The metallic particles in the sintered steel structures (S, S-Cu and S- Al_2O_3) are fused, while the ceramic particles remain as individual particles and hold the structure by capillary forces.

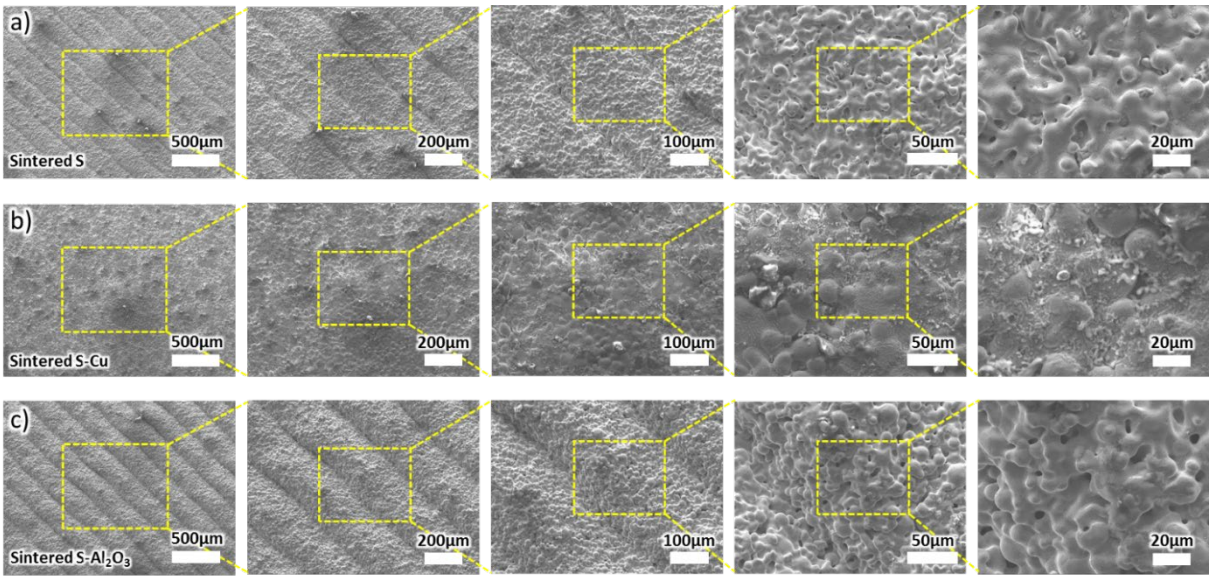

Figure S4. SEM images of the top layer of the fully dense sintered steel tensile bars: (a) sintered S, (b) sintered S-Cu, and (c) sintered S-Al_2O_3.

The sintered steel tensile bars are fully dense. The surface of sintered S-Cu is smoother than that of sintered S and sintered S-Al_2O_3.

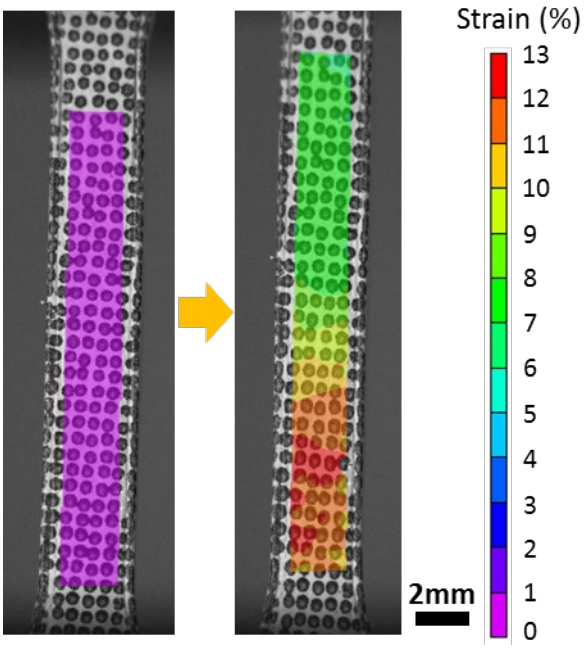

Figure S5. The strain distribution in the sintered steel tensile bars during tensile tests are measured through DIC. The tensile bar at the beginning of the tensile test (left) and close to failure (right).

Compared to extensometer, DIC can measure the strain more accurately. In addition, it can measure the strain distribution.

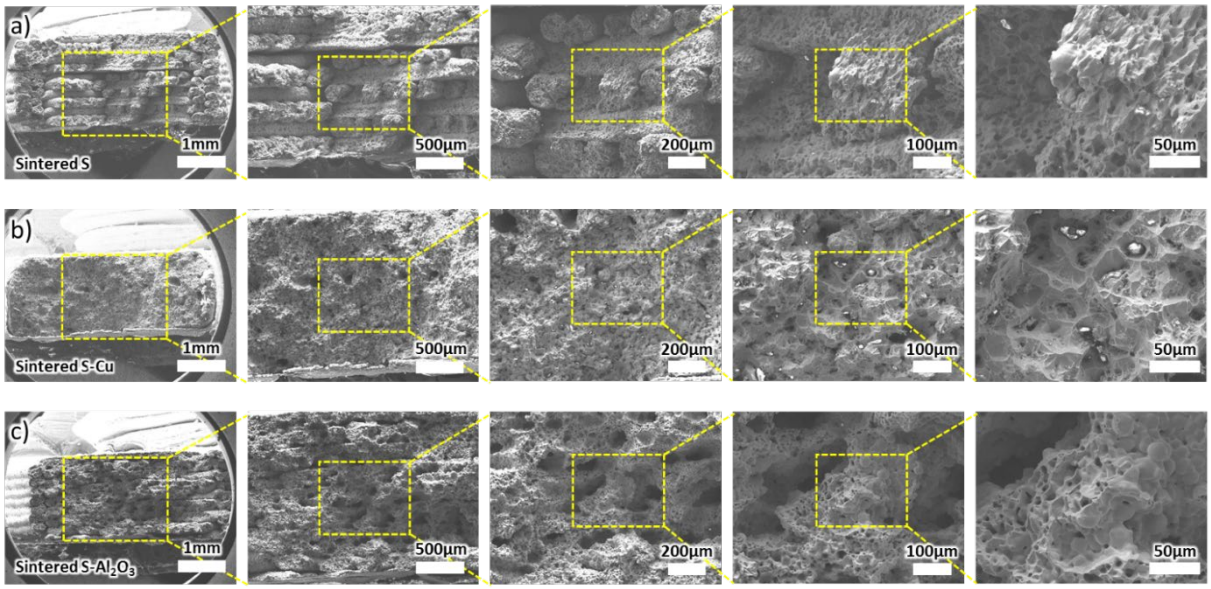

Figure S6. SEM images of the tensile fracture surfaces at different magnifications of (a) sintered S, (b) sintered S-Cu, and (c) sintered S-Al_2O_3.

The sintered S-Cu are denser and the filaments bond better than sintered S and S-Al_2O_3.

Table S1. Summary of the properties of the sintered steel structures.

	Sintered S	Sintered S-Cu	Sintered S-Al_2O_3
Linear size reduction (%)	11.2 ± 0.9	10.7 ± 1.1	11.0 ± 1.3
Micro surface roughness *Ra* (µm)	2.5 ± 0.5	1.6 ± 0.3	4.1 ± 1.2
Macro surface roughness *Ra* (µm)	4.9 ± 2.9	6.3 ± 2.5	13.9 ± 2.2
Volume percentage of iron (%)	97.8 ± 0.3	87.2 ± 1.8	98.1 ± 0.6
Volume percentage of copper (%)	0	10.4 ± 1.3	0
Filament porosity (%)	2.2 ± 0.3	2.4 ± 0.8	1.9 ± 0.6
Pore size (µm)	2.5 ± 0.8	3.0 ± 0.9	2.6 ± 1.0
Electrical conductivity (10^5 S/m)	7.4 ± 0.4	27.9 ± 4.2	6.9 ± 3.4
Young's modulus (GPa)	130 ± 6	174 ± 10	108 ± 6
Yield strength (MPa)	210 ± 4	284 ± 16	165 ± 8
Ultimate tensile strength (MPa)	359 ± 8	521 ± 57	304 ± 18
Elongation at failure (%)	8.7 ± 1.2	11.3 ± 3.6	10.1 ± 1.4

Video S1. The tensile test process with DIC measured strain showing on the sintered S sample.

Video S2. The tensile test process with DIC measured strain showing on the sintered S-Cu sample.

Video S3. The tensile test process with DIC measured strain showing on the sintered S-Al_2O_3 sample.